Theoretical Study on the Photoelectron Spectra of $Ln(COT)_2^-$: Lanthanide Dependence of the Metal-Ligand Interaction

Erika Nakajo, Tomohide Masuda, and Satoshi Yabushita

Department of Chemistry, Faculty of Science and Technology, Keio University, 3-14-1 Hiyoshi, Kohoku-ku, Yokohama 223-8522, Japan

Supporting Information

(S1) Resonance integral β of metal-ligand interaction

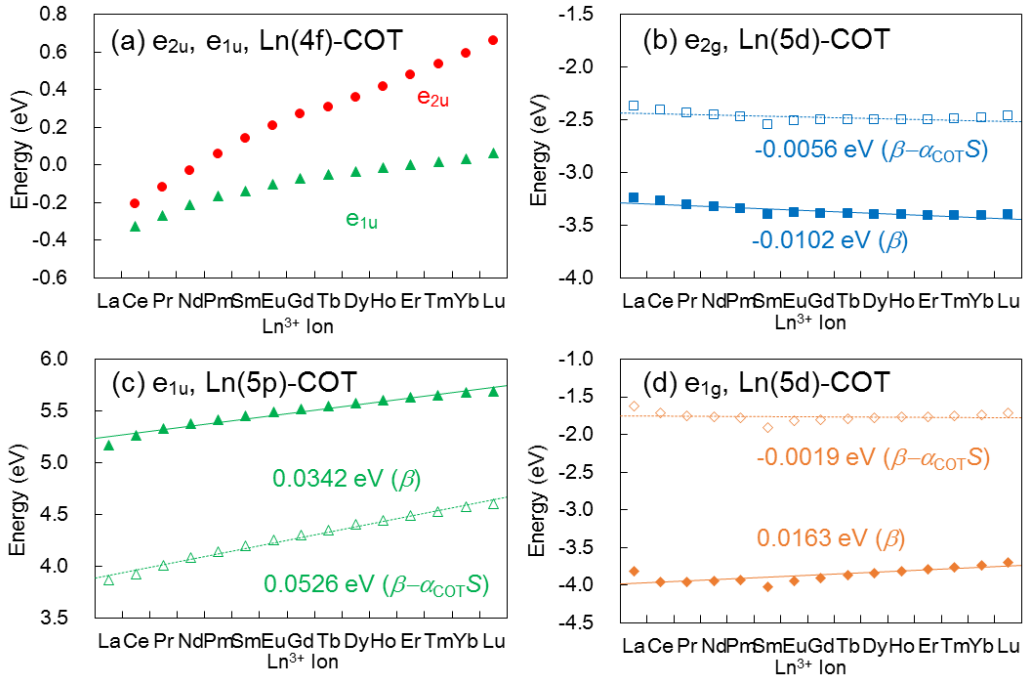

Figure S1. Values of β and β–$\alpha_{COT}S$ used in eq 4 calculated for (a) 4f-ligand interaction in the e_{2u} and e_{1u} MOs, (b) 5d-ligand interaction in the e_{2g} MO, (c) 5p-ligand interaction in the e_{1u} MO, and (d) 5d-ligand interaction in the e_{1g} MO. Each of the least squares fitted lines are presented along with the change rates. In panel (a), because of the small S values, the β–$\alpha_{COT}S$ values are essentially the same as the β values and are not shown.

Figure S1(a) shows a monotonic increase of β in the 4f-ligand interaction across the Ln series. On an average, these β values are one order of magnitude smaller than those for the 5d-ligand

(Figures S1(b) and (d)) and 5p-ligand (Figure S1(c)) interactions. The compactness of the 4f orbitals and the small 4f-ligand overlap result in the sign change in the β values, even though the energy order of π > 4f remains through the series.

(S2) MCQDPT2 energy levels and their splitting patterns for the whole series of Ln complexes

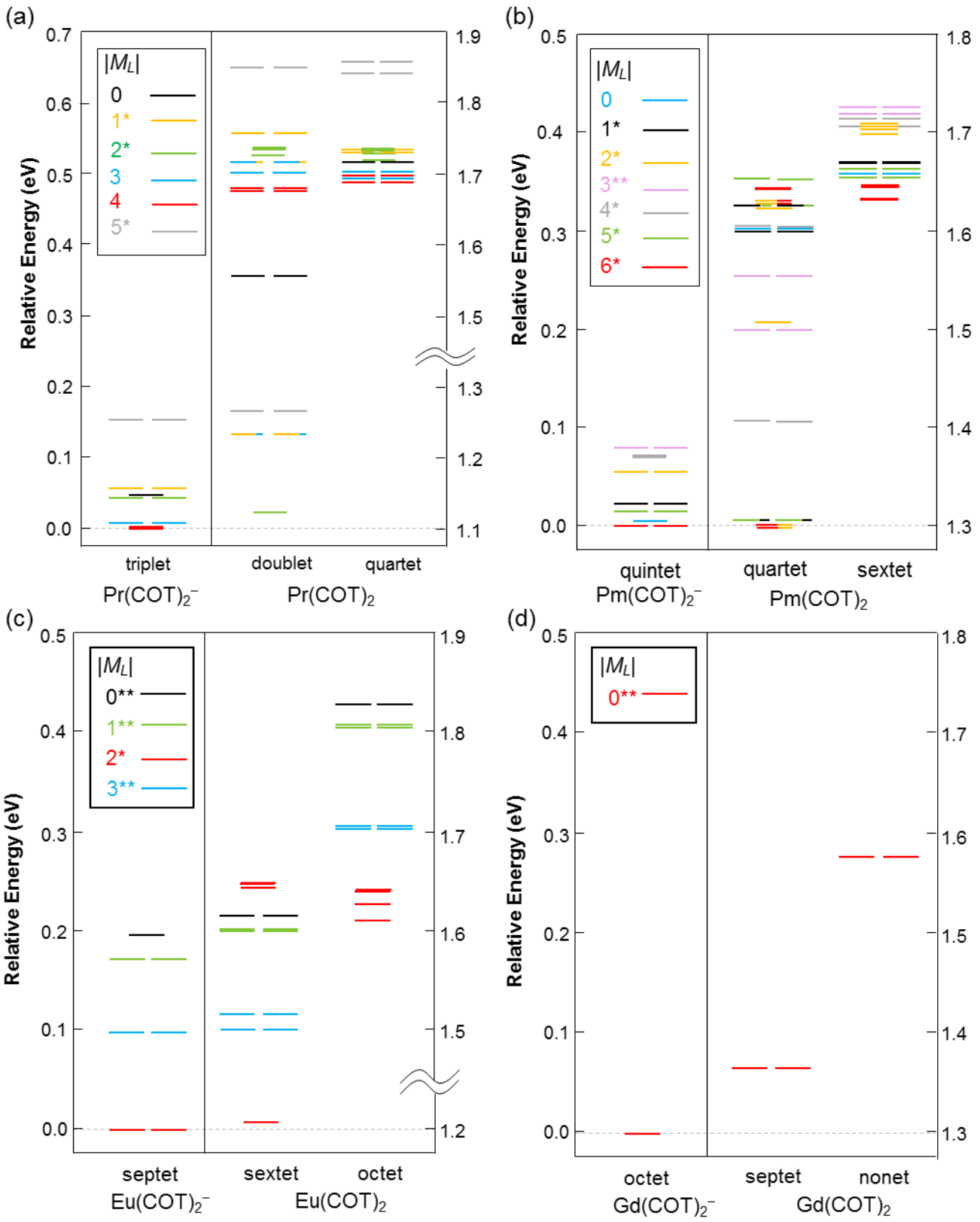

Figure S2. MCQDPT2 energy levels for (a) Pr ($4f^2$), (b) Pm ($4f^4$), (c) Eu ($4f^6$), and (d) Gd ($4f^7$) complexes.

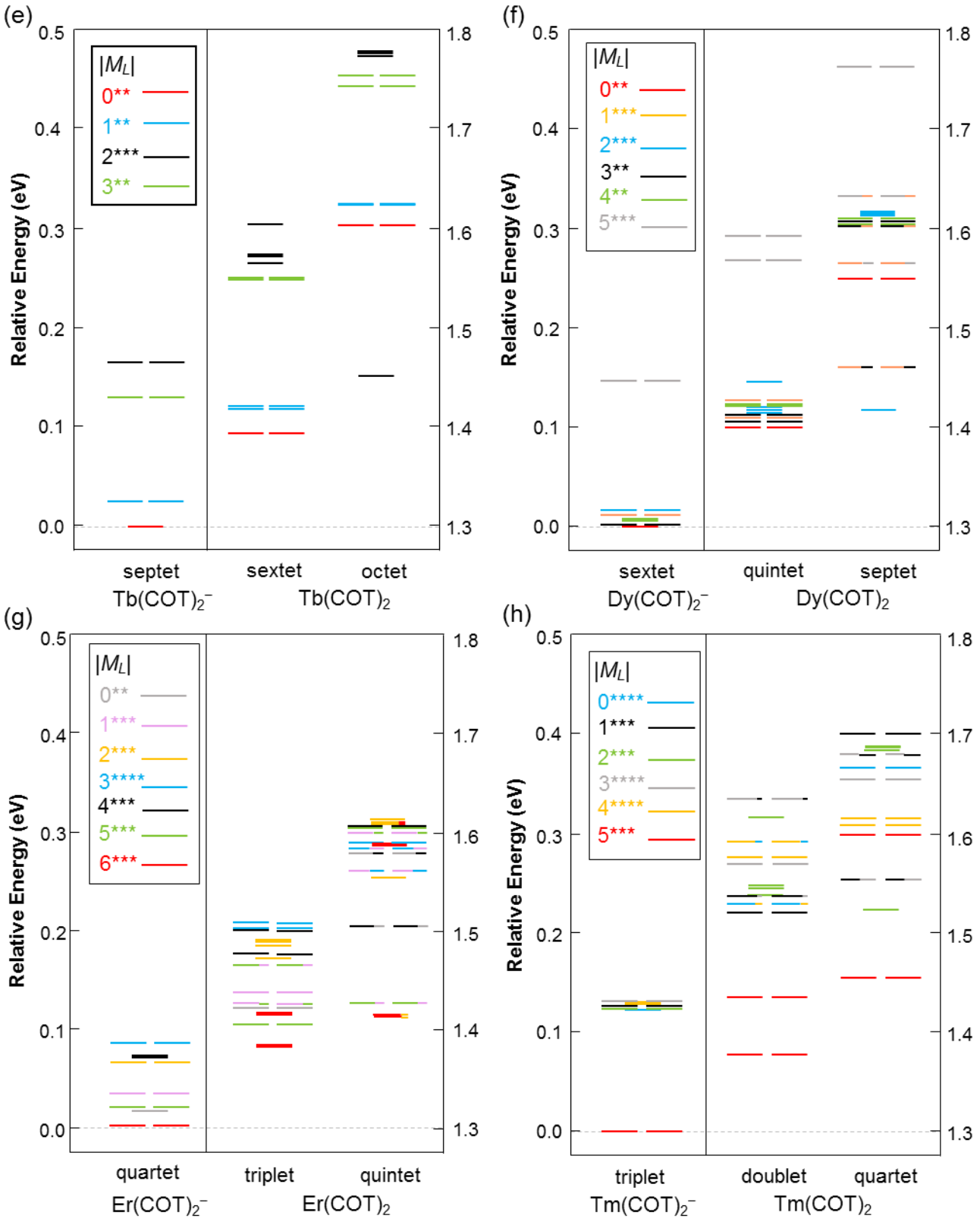

Figure S2 (Continued.) MCQDPT2 energy levels for (e) Tb ($4f^8$), (f) Dy ($4f^9$), (g) Er ($4f^{11}$), and (h) Tm ($4f^{12}$) complexes.

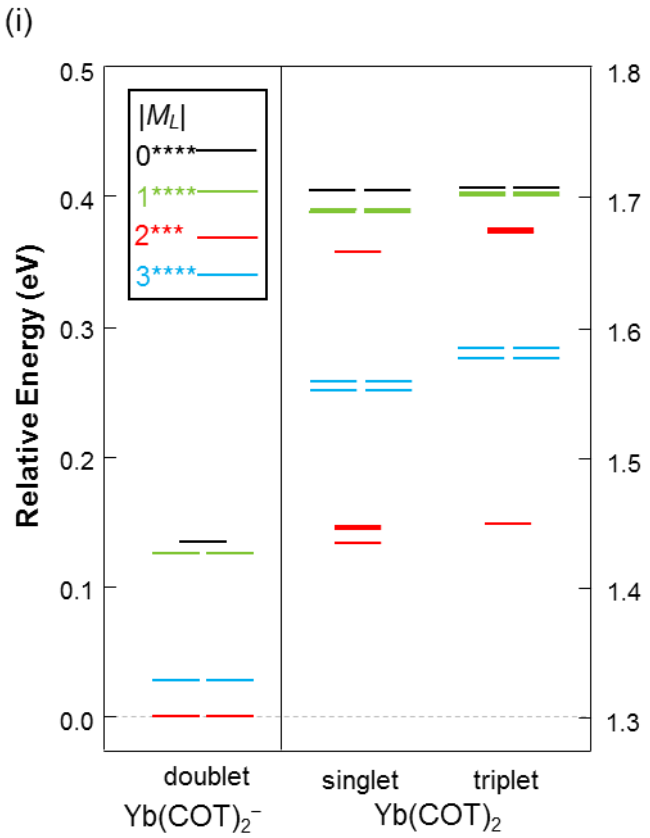

Figure S2 (Continued.) MCQDPT2 energy levels for (i) Yb ($4f^{13}$) complex.

As has been discussed in the text, the electronic structure of the Ln complexes is characterized by (i) the strong exchange interactions among the 4f electrons, (ii) the ligand field perturbation, and (iii) the relaxation effect of the $4f_{e2u}$ orbitals caused by the electron detachment from the anion π_{e2u} orbitals. This relaxation effect is expressed with the one-electron excitation configurations from the $4f_{e2u}$ to π_{e2u} orbitals belonging to the same symmetry. Note that the interactions (i) and (ii) appear in both anion and neutral complexes, and (iii) is inherent in the neutral complexes, and its magnitude is much smaller than that of (i). Since our discussion for the additional interaction (iii) is largely based on the perturbation method and group theory, a clear explanation of the electronic wave functions of the neutral complexes is in order now.

The spatial part of the electronic wave functions for the neutral complexes can be expressed as a linear combination of configurations denoted as $\Phi_{\Gamma_{else}} \cdot 4f_{e2u}^{p} \cdot \pi_{e2u}^{q}$, where $\Phi_{\Gamma_{else}}$ is a many-electron configuration excluding the one-electron $4f_{e2u}$ and π_{e2u} orbitals, and has the

specified irreducible representation (irrep) of Γ_{else}. Here, p and q are the orbital occupation numbers. Because of the stronger interaction (i) compared to (iii), the energy eigenstates are well described by the orbital coupling scheme of $(\Phi_{\Gamma_{\mathrm{else}}} 4\mathrm{f}_{\mathrm{e2u}}^{p}) \cdot \pi_{\mathrm{e2u}}^{q}$, however in the current problem with many degenerate one-electron orbitals, a different coupling scheme denoted as $\Phi_{\Gamma_{\mathrm{else}}} \cdot (4\mathrm{f}_{\mathrm{e2u}}^{p} \pi_{\mathrm{e2u}}^{q})$ is more convenient for the discussion of the above (iii) based on the symmetry classification of the $(4\mathrm{f}_{\mathrm{e2u}}^{p} \pi_{\mathrm{e2u}}^{q})$ configurations. Then, we first consider the degree of configuration mixing in the second coupling scheme, then with transforming the relevant configurations from the second to the first coupling scheme, we describe the energy splitting patterns. Those who are interested in more details may consult a classic reference book by Griffith,[79] on which our group theory terms are based.

The ϕ (angular coordinate) dependent part of the relevant one-electron wavefunctions is represented in the form of $\exp(im_l\phi)$ or a pair of $\cos(m_l\phi)$ and $\sin(m_l\phi)$. We generally prefer to use the latter real forms, since they transform as basis functions belonging to irreps of D_8 or D_{8h} point group. To make the following discussion more concrete, the spatial configurations are occasionally expressed by combining only the ϕ dependent parts of the $4\mathrm{f}_{\mathrm{else}}$, $4\mathrm{f}_{\mathrm{e2u}}$, π_{e2u} functions, with defining their respective angular coordinates as ϕ_1, ϕ_2, and ϕ_3. In what follows, the axial angular momentum of the total system and that of the $4\mathrm{f}_{\mathrm{else}}$ component are denoted as $M_{L,\mathrm{total}}$ and $M_{L,\mathrm{else}}$, respectively.

Let us first consider the case of $(4\mathrm{f}_{\mathrm{e2u}})^1(\pi_{\mathrm{e2u}})^3$ configuration in Figure 8 (a) in the above second coupling scheme. The coupling between the $4\mathrm{f}_{\mathrm{e2u}}$ and π_{e2u} orbitals results in four states with the ϕ dependence of $\cos(2\phi_2-2\phi_3)$, $\sin(2\phi_2-2\phi_3)$, $\cos(2\phi_2+2\phi_3)$, and $\sin(2\phi_2+2\phi_3)$, belonging to A_1, A_2, B_1, and B_2 irreps, respectively. From their ϕ dependence, it is clear that the A_1, A_2, B_1, and B_2 components change the axial angular momentum $M_{L,\mathrm{else}}$ by 0,0, ±4, and ±4 units, respectively.

As shown in Figure 8(b), if Γ_{else}, the irrep excluding $(4\mathrm{f}_{\mathrm{e2u}}, \pi_{\mathrm{e2u}})$, belongs to A_1 or A_2, then $M_{L,\mathrm{total}}=M_{L,\mathrm{e2u}}$, and the splitting pattern is similar to that obtained with ignoring the $4\mathrm{f}_{\mathrm{else}}$ part, while if Γ_{else} is one of E_1, E_2, E_3, and $(\mathrm{B}_1, \mathrm{B}_2)$, a different splitting pattern appears. The latter case is now explained taking the $|M_L|=5$ case ($(4\mathrm{f}_{\mathrm{e3u}})^1(4\mathrm{f}_{\mathrm{e2u}})^1$, $\Gamma_{\mathrm{else}}=\mathrm{E}_3$, grey level) of the Pr negative complex

(Figure S2 (a)) as an example. In this case, the neutral complex has two values of $M_{L,\mathrm{total}}$=5+2=7 ($((E_3\times E_2)^{E3}\times E_2)=E_1$) and 5-2=3 ($((E_3\times E_2)^{E3}\times E_2)=E_3$). In these first coupling schemes, the direct products of three irreps are denoted as $(\Gamma_1\times\Gamma_2)^{\Gamma12}\times\Gamma_3$. In the second coupling scheme, the former E_1 level is considered to be derived by the coupling of $M_{L,\mathrm{else}}$ (=3)+4, that is, $E_3\times(E_2\times E_2)^{B1,B2}=E_1$ in the direct product scheme of $\Gamma_1\times(\Gamma_2\times\Gamma_3)^{\Gamma23}$. Since neither B_1 nor B_2 component does not have interaction with the Ln^{4+} configuration, no stabilization energy appears in the doublet E_1 level (gray) in Figure S2 (a)), but significant energy lowering can be seen in the doublet E_3 level (gray).

To examine the latter doublet E_3 state, their configuration functions are explicitly written down in the two coupling schemes, $(E_3\times E_2)^{E3}\times E_2=E_3$ and $E_3\times(E_2\times E_2)^{A1,A2}=E_3$. Referring to reference 79, the former configuration functions with cosine component is given as follows,

$$((E_3\times E_2)^{E_3}\times E_2)_c^{E_3}=(E_3\times E_2)_c^{E_3}E_{2c}-(E_3\times E_2)_s^{E_3}E_{2s}$$
$$=\cos(3\phi_1+2\phi_2)\cos 2\phi_3+\sin(3\phi_1+2\phi_2)\sin 2\phi_3.$$

As is easily confirmed, the above expression is just equal to the sum of the following two configuration functions in the second coupling scheme,

$$(E_3\times(E_2\times E_2)^{A_1})_c^{E_3}=\cos 3\phi_1\times\cos(2\phi_2-2\phi_3)$$
$$(E_3\times(E_2\times E_2)^{A_2})_c^{E_3}=-\sin 3\phi_1\times\sin(2\phi_2-2\phi_3).$$

The analysis so far states that the E_3 state in the first coupling scheme is composed of both the $\Gamma_{e2u}=A_1$ and A_2 intermediate components in the second coupling scheme, thus the energy is approximately given as their average energy. Since only the $\Gamma_{e2u}=A_1$ component can involve the mixing with the Ln^{4+} configuration, the low-spin E_3 states are stabilized, and the stabilization energy is decreased by a half because of the mixing with the non-stabilized $\Gamma_{e2u}=A_2$ component. In the actual calculations, the weights of the $\Gamma_{e2u}=A_1$ and A_2 components deviate from 1:1 because of the interactions with other states having the same overall irrep E_3. Anyway, if Γ_{else} belongs to doubly degenerate irreps, one can expect the splitting pattern shown on the right-hand side of Figure 8 (b).

A similar explanation can be applied to the states with $(4f_{e2u})^3(\pi_{e2u})^3$ configuration. In this case, Γ_{e2u} is one of A_1, A_2, B_1, and B_2 again, and as explained in the text, if Γ_{else} belongs to A_1 or A_2, the coupling of the $4f_{e2u}$ and π_{e2u} orbitals gives the splitting pattern shown on the left-hand side of Figure 8 (g). As the second coupling scheme suggests that the low-spin configurations with $\Gamma_{e2u}=A_1$, B_1, and B_2 involve the mixing with the Ln^{4+} configuration, the states with $M_{L,\text{total}}=M_{L,\text{else}}$ and $M_{L,\text{else}}\pm4$ are all stabilized. As for the high-spin states, only the configurations with $\Gamma_{e2u}=A_2$ involve the mixing, thus the states with $M_{L,\text{total}}=M_{L,\text{else}}$ are stabilized. Consequently, if Γ_{else} belongs to one of E_1, E_2, E_3, and (B_1, B_2), the largest stabilizations occur in the low-spin states with $M_{L,\text{total}}=M_{L,\text{else}}\pm4$, and the stabilizations of about a half size occur in the low- and high-spin states with $M_{L,\text{total}}=M_{L,\text{else}}$. The high-spin states with $M_{L,\text{total}}=M_{L,\text{else}}\pm4$ show no stabilization due to the mixing with the Ln^{4+} configuration. These splitting patterns are shown in the right-hand panel of Figure 8(g)).

In contrast to the above two cases, the situation is quite simple for the $(4f_{e2u})^2(\pi_{e2u})^3$ configuration. The $4f_{e2u}$ orbitals are half-filled with parallel spins, and the irrep of the $(4f_{e2u})^2$ part is A_2. Thus, Γ_{e2u} is E_2, and the second coupling scheme $\Gamma_{else}\times(A_2\times E_2)^{E2}$ gives $M_{L,\text{total}}=M_{L,\text{else}}\pm2$ for the neutral complex. Because the A_2 component of the $(4f_{e2u})^2$ part has no ϕ_2 dependence, the configuration functions in the second coupling scheme are equivalent to those in the first coupling scheme $(\Gamma_{else}\times A_2)\times E_2$, and the angular momentum recoupling is not needed. Therefore, as the second coupling scheme shows, all the low-spin states are stabilized by the interaction with the Ln^{4+} configuration (Figure 8(d)).

(S3) Spin-orbit coupling (SOC) effect on the energy of the anion and neutral states

In general, SOC plays an important role for describing the electronic structure of Ln systems. This is especially true for the later Ln cases, in which the splitting energy levels due to the SOC is almost ten times larger than those caused by the ligand field for $Ln(COT)_2^-$, thus SOC should be taken into account for more precise description. However, as explained below, its inclusion has little effect on the vertical detachment energies and the X peak splittings. This is because both in the anion and neutral complexes with the strong ionic bonds, the 4f orbitals remain essentially as the atomic orbitals and their variations on photodetachment is negligibly small, therefore the SOC due to the open-shell 4f electrons remains the same. In what follow, we briefly explain this point using a simple degenerate first-order perturbation scheme.

Let L, S, M_L, and M_S denote the total orbital and spin angular momentum quantum numbers and their respective axial component quantum numbers of Ln^{3+} without the SOC, and also let J and M_J denote the total angular momentum quantum number and its z-component with the SOC. First, the SO coupled ground states of most Ln^{3+} ions are efficiently approximated using the L-S coupling scheme,[79] and $J=L-S$ ($n<7$) or $J=L+S$ ($n\geq 7$) depending on the number of f electrons n, and SO interaction within the COT portion is negligible. In this situation, the SO coupled wavefunction of the anion complex $Ln^{3+}(COT^{2-})_2^-$ with the ligand field split component of M_J is approximately expressed as a product of the wavefunctions for the Ln^{3+} and for the two COT ligands as follows,

$$\psi_{\text{anion}} = A \sum_{M_L+M_S=M_J} c^{\text{anion}}_{M_L,M_S} \phi(L,M_L,S,M_S)\cdot\phi(\pi_{\text{e2u}}{}^4), \tag{S1}$$

where A is the antisymmetrizer, and the expansion coefficints

$$c^{\text{anion}}_{M_L,M_S} = \left\langle L,M_L,S,M_S \,\middle|\, J,M_J \right\rangle \tag{S2}$$

are the Clebsch-Gordan coefficients for each component $\phi(L,M_L,S,M_S)$ of the Ln^{3+} ground state $^{2S+1}L_J$, and $\phi(\pi_{\text{e2u}}{}^4)$ symbolically stands for the two COT ligands. This is a good approximation for these weak field complexes. If only the first-order SOC is taken into account, and the second-order SO interactions are ignored for the ground LS term, the energy for (J, M_J) anion state as expressed in

(S1) is given as

$$E_{J,M_J}^{\text{anion}} = \langle \psi_{\text{anion}} | H^{\text{SF}} + H^{\text{SO}} | \psi_{\text{anion}} \rangle$$

$$= \sum_{M_L,M_S} \sum_{M_L',M_S'} c_{M_L,M_S}^{\text{anion}} c_{M_L',M_S'}^{\text{anion}} \langle L, M_L, S, M_S; \pi_{\text{e2u}}{}^4 | H^{\text{SF}} + H^{\text{SO}} | L, M_L', S, M_S'; \pi_{\text{e2u}}{}^4 \rangle$$

$$= \sum_{M_L,M_S} (c_{M_L,M_S}^{\text{anion}})^2 E(^{2S+1}L_{M_L}; \pi_{\text{e2u}}{}^4) + E_{\text{SO}}. \quad \text{(S3)}$$

Here, $E(^{2S+1}L_{M_L}; \pi_{\text{e2u}}{}^4)$ is the ligand field split energy without the SOC. E_{SO} represents the SOC energy, which is expressed in the well-known form as

$$E_{\text{SO}} = \frac{\lambda}{2}\left[J(J+1) - L(L+1) - S(S+1)\right]$$

$$= \begin{cases} -\lambda(L+1)S & (1 \le n \le 6) \\ +\lambda LS & (8 \le n \le 13). \end{cases} \quad \text{(S4)}$$

Here, λ is the SOC parameter. Eq. S3 shows that the SOC mixes electronic states with different M_L values, and it gives the averaged energy weighted by the square of the Clebsch-Gordan coefficients.

In a similar manner, the wavefunction of the SO coupled neutral state, whose Ln^{3+} portion is identical to that of the anion state $^{2S+1}L_J$ with the component of M_J is approximated with the same Clebsch-Gordan coefficients as follows,

$$\psi_{\text{neut}} = A \sum_{M_L+M_S=M_J} c_{M_L,M_S}^{\text{neut}} \phi(L, M_L, S, M_S) \cdot \phi(\pi_{\text{e2u}}{}^3), \quad \text{(S5)}$$

where

$$c_{M_L,M_S}^{\text{neut}} = \langle L, M_L, S, M_S | J, M_J \rangle. \quad \text{(S6)}$$

The energy for the neutral state is further expressed as

$$E_{J,M_J}^{\text{neut}} = \langle \psi_{\text{neut}} | H^{\text{SF}} + H^{\text{SO}} | \psi_{\text{neut}} \rangle$$

$$= \sum_{M_L,M_S} \sum_{M_L',M_S'} c_{M_L,M_S}^{\text{neut}} c_{M_L',M_S'}^{\text{neut}} \langle L, M_L, S, M_S; \pi_{\text{e2u}}{}^3 | H^{\text{SF}} + H^{\text{SO}} | L, M_L', S, M_S'; \pi_{\text{e2u}}{}^3 \rangle$$

$$= \sum_{M_L,M_S} (c_{M_L,M_S}^{\text{neut}})^2 \left[\frac{S}{2S+1} E_{M_L \pm 2}^{2S}(^{2S+1}L_{M_L}; \pi_{\text{e2u}}{}^3) + \frac{S+1}{2S+1} E_{M_L \pm 2}^{2S+2}(^{2S+1}L_{M_L}; \pi_{\text{e2u}}{}^3) \right] + E_{\text{SO}}. \quad \text{(S7)}$$

For the neutral state with SOC, the energy of the low-spin and high-spin states is averaged with the weighting factors of each spin multiplicity.

In these approximations given in eqs. S2, S3, S6 and S7, the anion and neutral complexes have identical SOC energy and the expansion coefficient. In the actual calculations, however, their values should be slightly different for the anion and neutral complexes. The small differences of these values are a consequnce that the electronic structure of the Ln complexes is dominated by ionic bond within the weak ligand field regime and that the SOC effect of the ligand portion is negligibly small. In other words, for the anion and neutral states having the same 4f configuration, the SOC causes a similar energy shift and has an insignificant effect on the vertical detachment energy, which is the energy difference between the anion and neutral states. Although the absolute values of SOC are typically larger than the ligand field perturbation, and the splitting pattern becomes more complicated with the SOC, the coulombic interaction between the $4f_{e2u}$ and ligand π_{e2u} electrons, which is a second-order interaction not included in the above first-order model, still plays the dominating role in the splitting of the X peaks.

(S4) Basis set dependence of orbital interaction analysis

Mulliken population analysis, which estimates atomic charges by partitioning the wave function in terms of the basis functions, has a shortcoming in that the final results show a rather large basis-set dependence. In particular, diffuse functions added to improve the wave function often give results inconsistent with the chemical intuition and cause a problem in the interpretation. We faced several problems in our orbital interaction analysis. After some trial and error analyses, we have slightly modified the basis functions from the originally optimized one by Cundari and Stevens [65] (denoted CS basis set) as detailed below.

For example, the $5p_{e1u}$ orbital contributes to the e_{1u} MO in an anti-bonding manner (Figure 2), however, we have also found the most diffuse p-type primitive basis function contributed to the e_{1u} MO in an in-phase manner. Since the diffuse function has only a small chemical impact to the

Ln^{3+} 5p orbital, we have removed the most diffuse sp-type functions from the CS basis set. Figure S3 compares the 5p-ligand overlap calculated using the original CS basis sets and the new basis sets (denoted 5p-like basis sets). The overlap calculated with the CS basis sets shows a drastic change due to the increasing contribution of the diffuse p-type function across the Ln series. However, this significant change is actually not relevant to the 5p-ligand interaction. These 5p-like basis sets were used to calculate the radial expectation value of the 5p orbital (Figure 4), overlap between the π_{e1u} and $5p_{e1u}$ orbitals (Figure 5(a)), the interligand overlap in the e_{1u} MO (Figure 5(b)), the energy of the π_{e1u} orbital (Figure 6(c)) and the $5p_{e1u}$ orbitals (Figure 6(g)), and β (Figure S1(c)).

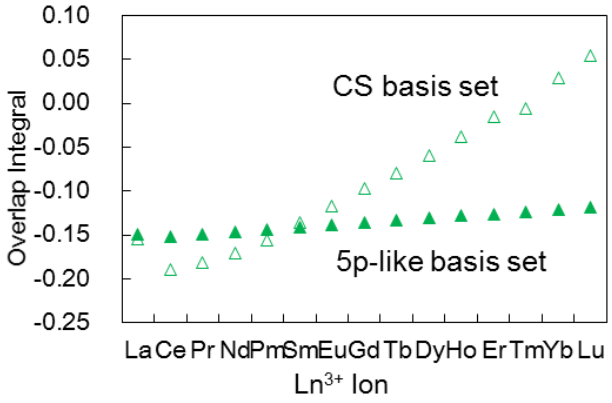

Figure S3. Overlap integral between the π_{e1u} and $5p_{e1u}$ orbitals in the e_{1u} MO calculated using the CS basis sets and the 5p-like basis sets.

The diffuse basis functions used for the 5d and 4f atomic orbitals of Ln are even more problematic, because they significantly contribute to the atomic orbitals of Ln^{3+}. Figure S4 shows the energies of the $5d_{e2g}$ and $5d_{e1g}$ orbitals, calculated with the CS basis sets. In the e_{1g} MO case, the diffuse d-type function is directed at the ligands and effectively used to describe the ligand orbital. It results in the over-stabilization of the $5d_{e1g}$ orbital, and the basis set modification is needed. We contracted the d-type primitive functions of the CS basis sets into the single-zeta 5d atomic orbital of Ln^{3+} and constructed the (9s9p5d)/[4s4p1d] basis set for La and the (6s6p3d7f)/[4s4p1d2f] basis sets for Ce-Lu. We used these 5d-like basis sets to calculate the radial expectation value of the 5d orbital

(Figure 4), the 5d-ligand overlap (Figure 5(a)), the interligand overlap in the e_{2g} and e_{1g} MOs (Figure 5(b)), the energy of the π_{e2g} and π_{e1g} orbitals (Figures 6(b) and (d)) and the 5d orbitals (Figure 6(f)), and β (Figures S1(b) and (d)).

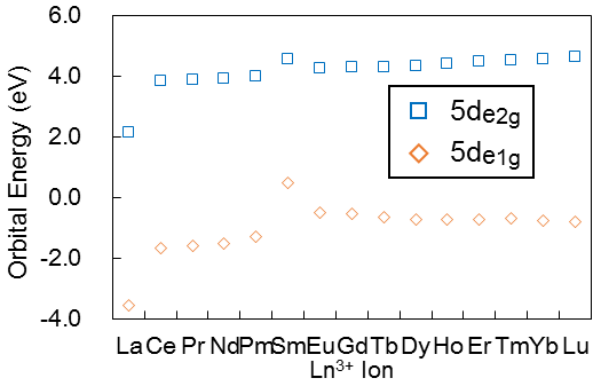

Figure S4. The energies of the $5d_{e2g}$ and $5d_{e1g}$ orbitals calculated using the CS basis sets.

As in the previous single-zeta 5d basis set, the single-zeta 4f basis sets (6s6p3d7f)/[4s4p2d1f] for Ce-Lu can be generated by contracting the f-type primitive functions into the single-zeta 4f orbital of Ln^{3+}. Since the contribution of the f-type functions to the MO is very small, our analysis on the 4f-ligand orbital interaction depends critically on the presence/absence of diffuse f-type functions. Figure S5 compares the 4f-ligand overlap calculated with the 4f-like basis sets and the CS basis sets. The overlap calculated using the 4f-like basis sets shows almost a steady decrease across the Ln series, reflecting the contraction of the 4f orbitals. On the other hand, the overlap calculated with the CS basis sets shows a discontinuous variation between Pm and Tb, which is attributed to the nonsystematic change of the diffuse f-type basis function. In this case, the Ln dependence of the overlap is clearly dominated by that of the most diffuse f-type primitive function (Figure S6). Therefore, our orbital interaction analysis has been carried out with the 4f-like basis sets (4f-ligand overlap (Figure 5(a)) and β (Figure S1(a))). However, since the single-zeta basis set is not flexible enough to describe electron correlation effect, we adopted the CS basis sets to estimate the many-body 4f-ligand interaction in 3-2. It is noted that, as shown in Table S1, the basis set dependence of the peak splitting energy was not so critical as it was for the 4f-ligand overlap

integral.

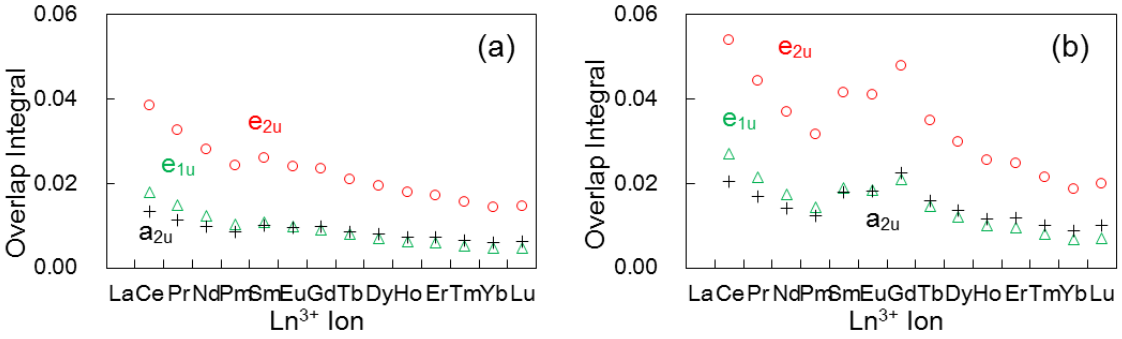

Figure S5. 4f-ligand overlap in the e_{2u}, e_{1u} and a_{2u} MOs, calculated using (a) 4f-like basis sets (the same as shown in Figure 5(a)) and (b) CS basis sets.

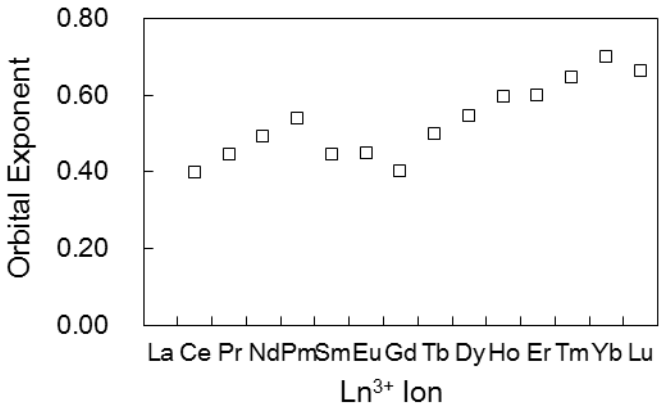

Figure S6. Smallest exponents of the f-type primitive functions used in the CS basis sets.

Table S1. Total energy and orbital energy and metal-ligand overlap in the e_{2u} MO for $Gd(COT)_2^-$, calculated using the CS basis sets and the 4f-like basis sets. The splitting value of the X peak by the MCQDPT2 method is also given. The 4f-ligand overlap decreased by half in the 4f-like basis sets, whereas the splitting value decreased about 20%.

	total energy (eV)	e_{2u} MO energy (eV)	π_{e2u} -4f $_{e2u}$ overlap	peak splitting (eV)
CS basis set	-19727.171	-2.261	0.048	0.215
4f-like basis set	-19727.031	-2.231	0.024	0.176